Immobilization of Chromium in Stainless Steel Slag Using Low Zinc Electric Arc Furnace Dusts

YONG LIN, BAIJUN YAN, TIMO FABRITIUS, and QIFENG SHU

A new synergistic treatment of stainless steel slag and low zinc content electric arc furnace (EAF) dusts is proposed to immobilize harmful chromium in stainless steel slag. The effects of $ZnFe_2O_4$ addition on the mineralogic phase and chromium leachability of CaO-SiO_2-MgO-Al_2O_3-Cr_2O_3 synthetic slag were investigated to explore the feasibility of this method. The mineralogic phases in stainless steel slag were investigated by scanning microscopy equipped with energy-dispersive spectroscopy and X-ray diffraction. The leaching concentration values of chromium and zinc were evaluated according to an alkaline digestion for the hexavalent chromium (US-EPA-3060A) and toxicity characteristic leaching procedure (TCLP, US-EPA-1311) method, respectively. It was found that all synthetic slags mainly contain α-Ca_2SiO_4, merwinite and spinel phase, in line with the calculation results by FactSage. The crystallization of spinel and merwinite phases was enhanced by the addition of $ZnFe_2O_4$ but suppressed the precipitation of α-Ca_2SiO_4. It was revealed that the leaching concentration of chromium was depressed by adding $ZnFe_2O_4$ and was far below the chemical limits defined in the French proposal for a criterion and evaluation methods for waste ecotoxicity (0.1 mg L^{-1}). In addition, the zinc leaching concentration meets the sanitary landfill standard. The proposed synergistic treatment method was further validated on industrial stainless steel slags and EAF dusts. Experimental results indicated that the synergistic treatment method can immobilize chromium effectively and the final slags can be disposed of by sanitary landfilling or recycling as constructional materials. A schematic technologic route diagram of the synergistic treatment was also proposed.

https://doi.org/10.1007/s11663-020-01777-0

I. INTRODUCTION

SIGNIFICANT amounts of stainless steel slag that contain harmful chromium are generated during stainless steel production.[1] For a long time, the massive amounts of stainless steel slag were land-filled or stored in slag yards as hazardous solid waste (waste category in China: HW21), which not only occupied a large amount of land but also polluted the natural environment. Previous studies[2] have shown that trivalent chromium in unstable phases among the stainless steel slag could be converted into highly toxic hexavalent chromium in air and aggravated in acidic oxygen-rich condition. Continuous leaching of hexavalent chromium can contaminate the surrounding environment, such as soil and underground water.[2] Therefore, stainless steel slag must be treated harmlessly before being reused or released to the environment.

The utilization of stainless steel slag must take its disintegration behavior, volume stability and especially the leachability into account. The disintegration behavior and volume stability are mainly caused by the transition from β-Ca_2SiO_4 (monoclinic) to γ-Ca_2SiO_4 (orthorhombic) accompanied by a volume expansion (approximately 12 pct)[3] or the hydration process of f-CaO and f-MgO.[4] The leachability[5] refers to the leaching ability of hazardous elements such as chromium and nickel during the storage or recycling as construction materials. Immobilization treatment can effectively reduce the leachability of heavy metals by converting them into chemically stable mineralogic phases, such as the spinel and glass phases, which are resistant to dissolution.[6,7] Hence, the immobilization of chromium in stainless steel slag has been investigated by many researchers.[8–15] Romero-Serrano *et al.*[8] reported that chromium leaching was suppressed by adding MgO

YONG LIN and BAIJUN YAN are with the School of Metallurgical and Ecological Engineering, University of Science and Technology Beijing, Beijing, 100083, P.R. China. Contact e-mail: baijunyan@ustb.edu.cn TIMO FABRITIUS is with the Process Metallurgy Research Unit, University of Oulu, 90014 Oulu, Finland. QIFENG SHU is with the School of Metallurgical and Ecological Engineering, University of Science and Technology Beijing and also with the Process Metallurgy Research Unit, University of Oulu. Contact e-mails: shuqifeng@gmail.com, qifeng.shu@oulu.fi

Manuscript submitted September 30, 2019.
Article published online January 24, 2020.

to the CaO-SiO_2-Cr_2O_3 system, which was attributed to stable binding of chromium in the $MgCr_2O_4$ phase. They also found that the addition of $FeSO_4$ and FeS_2 had positive effects on the immobilization of chromium.[9] Albertsson *et al.*[10,11] indicated that slow cooling, low oxygen partial pressure and low slag basicity (1.0 to 1.4) can improve the spinel phase precipitation. Shu *et al.*[12] found that the size of the spinel phase increased with increasing MnO content and decreasing CaO/SiO_2 ratio. However, disintegration was found in samples with a high MnO content and CaO/SiO_2 ratio. In addition, adding a certain amount of Al_2O_3,[13] FeO[14] or alumina-rich by-product[15] does in fact suppress the level of chromium leaching.

However, end-of-life galvanized steel products are commonly collected as scrap and re-melted in EAFs for steel recycling. During the melting process, zinc-containing EAF dusts are generated because of the bubble bursting at the liquid steel surface[16] and the relatively low boiling point of zinc (1180 K).[17] Approximately 15 to 20 kg of EAF dusts is generated for 1 ton of steel production.[18] Various operating conditions such as the characteristics of scraps, operating period and specification of the steel produced, *etc*., could affect the EAF duct composition.[17] However, it is accepted that EAF dusts generally consisted of zinc, iron, lead, cadmium, halides and other hazardous elements.[18,19] Owing to its physical and chemical properties, EAF dusts have been categorized as hazardous wastes by various government agencies (waste category in China: HW23). Several different methods have been proposed for recycling of EAF dusts, including pyrometallurgical, hydrometallurgical and hybrid processes (thermal reduction followed by leaching), which are mainly proposed to extract crude zinc from EAF dusts rich in ZnO.[17,20–27] However, most Chinese steel electrical arc furnaces produce steel using scrap steels combined with a certain amount of liquid metal, so the zinc content in EAF dusts is relatively low (< 10 pct[28]) compared with other countries (> 20 pct[23,24,27]). The economic benefit of recovering zinc from low-zinc-content EAF dusts is limited. Therefore, most EAF dusts are not utilized in China.

In the present work, we proposed a synergistic treatment method using stainless steel slag and low-zinc-content EAF dusts. This method is mainly based on the promotion of crystal growth of spinel by the main component, $ZnFe_2O_4$, in EAF dusts. To verify the feasibility of this method, the effects of $ZnFe_2O_4$ addition on mineralogic phases and Cr leachability in CaO-SiO_2-MgO-Al_2O_3-Cr_2O_3 synthetic slag were first investigated. The mineralogic phases in synthetic stainless steel slag with and without $ZnFe_2O_4$ addition were characterized by scanning microscopy equipped with energy-dispersive spectroscopy (SEM-EDS) and X-ray diffraction (XRD). The leaching concentrations of chromium and zinc were also evaluated according to the US-EPA-3060A[29] and TCLP method 1311,[30] respectively. Then, the validation of the synergistic treatment method was performed on industrial stainless steel slag and EAF dusts under similar conditions. Finally, a technologic route for the synergistic treatment method was proposed.

II. MATERIALS AND METHODS

A. *Sample Preparation*

The synthetic slag samples were prepared with reagent-grade powder (CaO, SiO_2, MgO, Al_2O_3, Cr_2O_3 and $ZnFe_2O_4$). CaO was obtained by calcining $CaCO_3$ at 1373 K for 6 h in a muffle furnace. MgO was also calcined at 1273 K in a muffle furnace for 6 h to decompose any hydroxide and carbonate. SiO_2, Al_2O_3, Cr_2O_3 and $ZnFe_2O_4$ were dried at 393 K in an oven for 4 h to remove moisture. Table I presents the chemical composition of the original slag samples. After thoroughly mixing the chemicals in an agate mortar, the powder mixtures were pressed into 20-mm-diamter pellets. The prepared samples were preserved in a desiccator to minimize re-absorption of moisture and carbon dioxide from the atmosphere.

Industrial slag from EAF of stainless steelmaking was obtained from a Chinese steelwork. EAF dusts were collected from a bag filter system in another Chinese steelwork. The chemical compositions of industrial stainless steel slag and EAF dusts characterized by X-ray fluorescence (XRF) are listed in Tables II and III, respectively. The content of Cr_2O_3 in stainless steel slag is 3.88 wt pct, while Fe_2O_3 is the dominant component in EAF dusts coexisting with 6.35 wt pct ZnO. Some heavy metal elements (Pb) and halogen elements (Cl) were also detected in EAF dusts. Most mineralogic phases of industrial stainless steel slag were determined by XRD to be γ-dicalcium silicate, merwinite, akermanite, magnesiochromite, cuspidine and periclase, as shown in Figure 1. EAF dusts mainly consist of magnetite, zinc ferrite and zinc oxide. For validation on industrial materials, the stainless steel slag and EAF dusts were mixed thoroughly with a mass ratio of 4/1. To emphasize the function of synergistic treatment, a stainless steel slag sample without EAF dust addition was set as a blank experiment.

B. *Melting and Heat Treatment*

The melting, cooling and heat treatment of synthetic and industrial samples were performed in a vertical tube furnace with molybdenum silicide as heating element. The samples were contained in molybdenum crucibles and positioned in the even temperature zone of the furnace. High-purity argon gas (99.999 pct) was employed to maintain an inert atmosphere to prevent the oxidation of molybdenum crucibles. All samples underwent the same heat treatment regime. The furnace was then heated at a heating rate of 5 K min^{-1} with the argon flow rate of 300 mL min^{-1}. The samples were first heated to 1873 K and then held for 30 min to eliminate bubbles and homogenize its chemical composition. After that, the samples were cooled to 1673 K at a cooling rate of 5 K min^{-1} and then held for 120 min to crystallize isothermally. Finally, the samples were quenched by pulling them out of furnace and quickly dipping them into water, and then the samples were dried at 393 K in an oven overnight.

Table I. Chemical Compositions of Synthetic Slag Samples (Wt Pct)

Sample	CaO	SiO_2	MgO	Al_2O_3	Cr_2O_3	$ZnFe_2O_4$	R(CaO/SiO_2)	Total
1	48.00	32.00	8.00	6.00	6.00	0	1.5	100.00
2	46.80	31.20	8.00	6.00	6.00	2.00	1.5	100.00
3	45.60	30.40	8.00	6.00	6.00	4.00	1.5	100.00

Table II. Chemical Composition of Industrial Stainless Steel Slag (Wt Pct)

	CaO	SiO_2	Al_2O_3	Fe_2O_3	MgO	MnO	Cr_2O_3	F	S	Others
Stainless Steel Slag	49.45	31.25	3.94	1.58	6.14	0.72	3.88	1.75	0.37	0.92

Table III. Chemical Composition of EAF Dust (Wt Pct)

	Fe_2O_3	CaO	MgO	ZnO	K_2O	SiO_2	S	Na_2O	Cl	MnO	Pb	Others
EAF Dusts	38.94	25.32	8.73	6.35	4.27	3.66	3.39	3.00	2.13	1.29	0.79	2.13

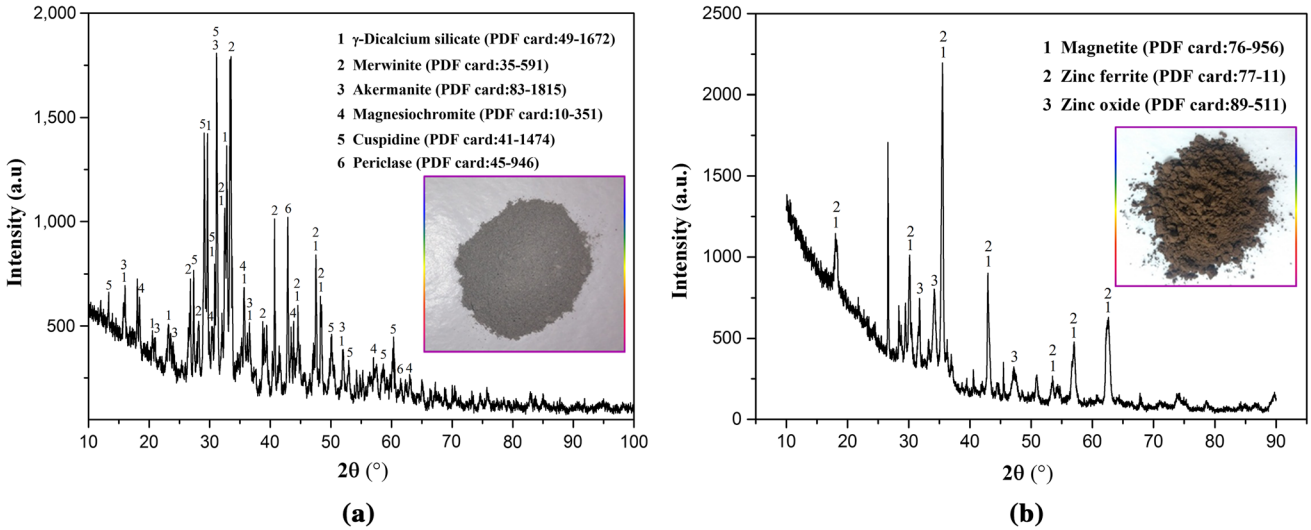

Fig. 1—XRD patterns and morphologies of (*a*) industrial stainless steel slag and (*b*) EAF dusts.

C. *Sample Characterization and Leaching Concentrations of Chromium and Zinc*

The quenched samples were subsequently separated from the molybdenum crucible. SEM-EDS and XRD were employed to investigate the mineralogic phases. For XRD analysis, some of the treated samples were crushed into fine powders with particle size < 100 mesh and then analyzed by a 18 kW X-ray diffractometer (model: RIGAKU TTRIII) with Cu-Ka radiation. SEM examinations were carried out using a FEI MLA 250 unit equipped with a Bruker SDD detector for EDS analysis. The working voltage was 20 kV. Before SEM-EDS examination, the samples were embedded in resin, ground, polished and coated with gold.

US-EPA-3060A method[29] was used to characterize the selective dissolution of Cr^{6+} from solid samples. According to the standard procedure, the alkaline digestion was carried out on 2.5 g samples. To completely digest samples, the particle size of each one was < 100 mesh. The fine powders were placed in a 250-mL beaker and mixed with 50 mL alkaline solution (0.28 M Na_2CO_3 and 0.5 M NaOH). The pH of the alkaline solution ranged from 11.8 to 12.3. Four hundred milligrams of anhydrous $MgCl_2$ and 0.5 mL 1.0 M phosphate solution (0.5 M K_2HPO_4 and 0.5 M KH_2PO_4) were also added to the beaker. The samples were stirred for at least 5 min without heating and then placed in a water bath to maintain the samples at 363 K to 368 K for at least 60 min with continuous stirring.

The suspensions were then filtered through 0.45-μm standard filter paper, and the filtrates were transferred to a 100-mL beaker. The pH of the solution was adjusted to 9.0 ± 0.5 by slowly adding 5.0 M HNO_3 solution with constant stirring. Finally, the Cr^{6+} content was detected by inductively coupled plasma-mass spectrometry (ICP-MS, ICAP RQ).

TCLP method 1311[30] is the most commonly used method to evaluate metal mobility in sanitary landfills. Thus, it was employed to evaluate the leaching concentration of zinc considering that zinc is a highly mobile element. For this purpose, 5 g sample with particle size < 100 mesh was placed in a borosilicate glass bottle together with 100 mL extraction fluid. The extraction fluid was prepared by glacial acetic acid and reagent water, whose pH was 2.88 ± 0.05 (extraction fluid #2). The mixture was then agitated at 30 rpm at 296 K. After 18 h leaching, the mixture was filtered through a new glass-fiber filter. The Zn concentration in the obtained filtrate was finally measured by inductively coupled plasma-optical emission spectrometric (ICP-OES, Agilent 5110DVD).

D. *Thermodynamic Calculation*

Thermodynamic simulations on phase precipitation during cooling of slags were performed by using FactSage software[31] (version 7.0), developed by Thermfact Ltd. (Montreal, Canada) and GTT-Technologies (Aachen, Germany). The phase precipitations during cooling of slags were calculated based on the FToxide database using the Scheil-Gulliver cooling model.[32] The reaction module and FToxide database were employed to calculate the formation Gibbs free energies of spinels within the temperature range of 673 K to 1973 K.

III. RESULTS AND DISCUSSION

A. *Effect of $ZnFe_2O_4$ Addition on Mineralogic Phases of Synthetic Stainless Steel Slag*

The laboratory-scale tests were performed with $ZnFe_2O_4$, which could cause volatilization problems. It is well known that ZnO has high vapor pressure and volatilizes easily at high temperature.[17] Therefore, vapor pressures of ZnO in slag samples were calculated by the following equations[33] to evaluate the volatilization of ZnO.

$$P_{ZnO} = a_{ZnO} P^*_{ZnO} \quad [1]$$

$$\log_{10} P^*_{ZnO} = A + \frac{B}{T} + C \log_{10} T + DT + ET^2 \quad [2]$$

where a_{ZnO}, P_{ZnO} and P^*_{ZnO} are the activity of ZnO in slag, vapor pressure of ZnO in slag and saturated vapor pressure of pure ZnO, respectively. The activity of ZnO in slag was calculated by FactSage. A, B, C, D and E in Eq. [2] are constants obtained from the Handbook of Vapor Pressure.[33] T is the temperature in Kelvin, T = 1873 K. The calculation results reveal that the vapor pressures of ZnO at 1873 K in sample 2 and 3 were 37.586 and 72.387 Pa, indicating that the loss of ZnO in slag due to volatilization was weak in this work.

The FactSage thermodynamic calculations of $ZnFe_2O_4$ modification at 1875 K to 1475 K are presented in Figure 2. The precipitation temperature of spinel phase is > 1875 K, and the total precipitation amount of the spinel phase increases slightly with increasing $ZnFe_2O_4$, approximately 10 pct. However, the precipitation temperature and the total precipitation amount of di-calcium silicate (Ca_2SiO_4) phase decrease significantly. By comparison, the effect of $ZnFe_2O_4$ addition on the precipitation temperature and mass percentage of precipitated merwinite ($Ca_3Mg(SiO_4)_2$) phase is not obvious. Gehlenite ($Ca_2(Mg,Al)Si_2O_7$) is precipitated at temperatures < 1675 K. These calculation results were compared with the experimental results.

SEM micrographs of synthetic stainless steel slags are presented in Figure 3. Chemical compositions of various mineralogic phases in quenched samples were determined by EDS and are summarized in Table IV. According to Figure 3 and Table IV, three crystalline phases were identified in all samples: di-calcium silicates, merwinite and spinel phase. XRD patterns of synthetic stainless steel slag are shown in Figure 4. Peaks of di-calcium silicates, merwinite and spinel phase were also found in the XRD patterns. The XRD results are in good accordance with the SEM and EDS results. It should be mentioned that there is a certain amount of Mg dissolution in the di-calcium silicate phase according to Table IV. The compositions determined by EDS for sample 1 and 2 are close to the composition of bredigite.[34–37] However, it is usually difficult to distinguish bredigite from α-Ca_2SiO_4 because these two minerals have very similar XRD patterns, as proposed by Bai *et al.*[38] and Segui *et al.*[34] Tilley and Vincent, who described and named this kind of mineral from Scawt Hill, Northern Ireland, proposed that bredigite was isostructural with α-Ca_2SiO_4.[35] It was proposed in later researches that bredigite is chemically and structurally distinct from α-Ca_2SiO_4.[37] Due to the controversy about the existence of bredigite, only di-calcium silicates were considered in the present work. The phases observed by SEM-EDS and XRD are in good agreement with the phases calculated by FactSage. Gehlenite was not found in the samples because the precipitation temperature was lower than the quenching temperature (1673 K).

Figure 5 presents the distribution of elements in each sample analyzed by EDS mapping. Table IV and Figure 5 show that the Cr element was mainly distributed in the spinel phase. The Zn element was mainly distributed in the spinel phase. There was also some Zn distribution in the glassy matrices. The Fe element was mainly distributed in the spinel phase and glassy matrices. There were fewer distributions of Fe in the α-dicalcium silicate and merwinite phases. The distributions of Zn and Cr in Ca_2SiO_4, spinel, liquid slag and $Ca_3MgSi_2O_8$ according to FactSage calculation and

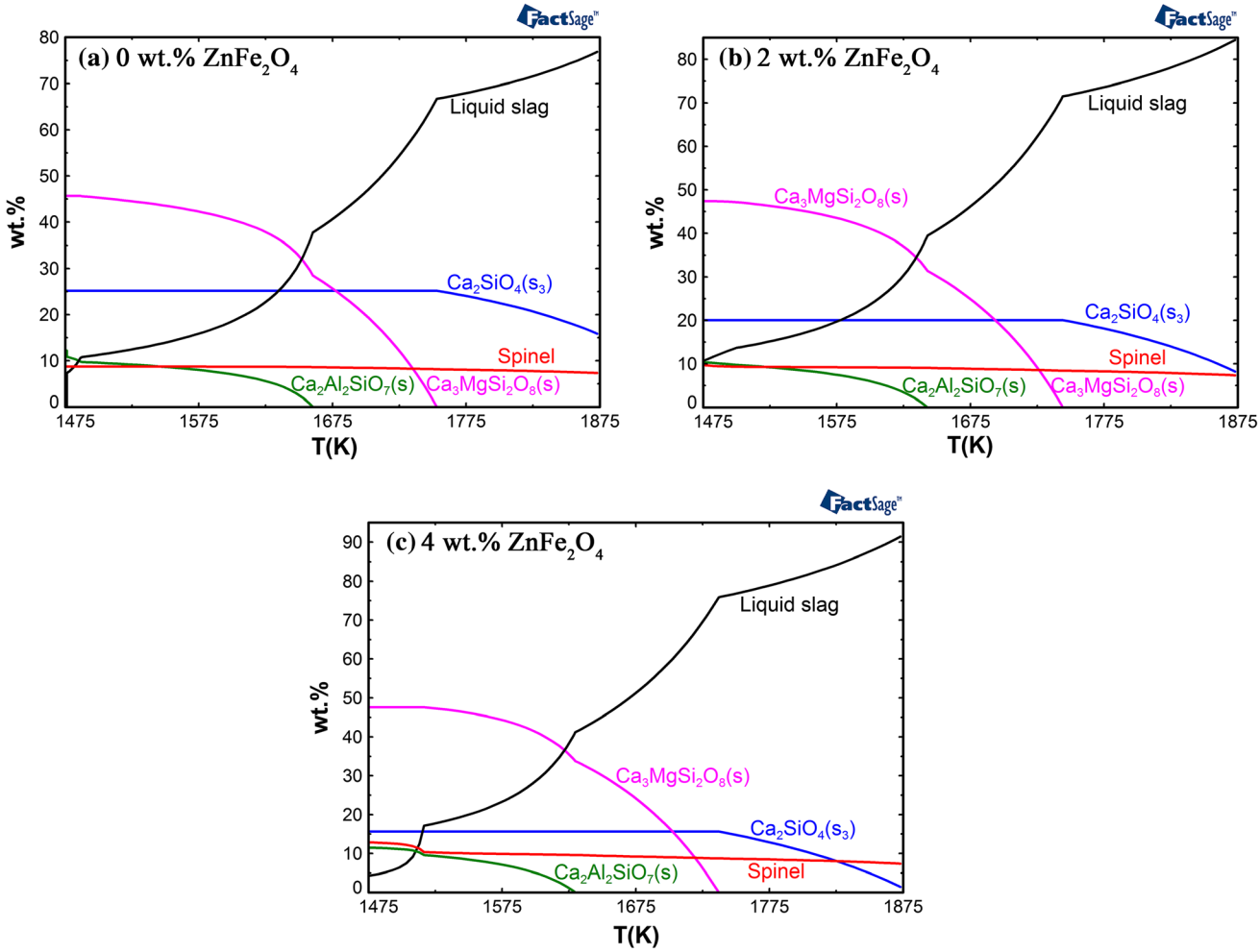

Fig. 2—Thermodynamic simulation results of phase precipitation during cooling of slags with various $ZnFe_2O_4$ additions using the Scheil-Gulliver model: (*a*) 0 wt pct $ZnFe_2O_4$; (*b*) 2 wt pct $ZnFe_2O_4$; (*c*) 4 wt pct $ZnFe_2O_4$.

EDS analysis are summarized in Table V. There are no dissolutions of Zn and Cr in $Ca_3MgSi_2O_8$ phase and Cr dissolution in Ca_2SiO_4 phase according to the FactSage results, which could be due to the limitation of the database. The contents of Cr in liquid slag from the FactSage results were much lower than those from the EDS results. The results of both FactSage and EDS showed that most Cr and Zn were concentrated in the spinel phase. The distribution of Zn in liquid slag increased from 0.653 pct to 1.256 pct according to the FactSage simulation, consistent with the EDS results.

The distribution of Zn and Fe in the spinel phase could be explained from viewpoints of thermodynamics and crystallography. Figure 6 lists the formation Gibbs free energies of binary spinels within the temperature range of 673 K to 1973 K according to FactSage calculation. Obviously, the formation Gibbs free energies of most binary spinels are negative. This result is consistent with the study of Tathavakar.[39] Actually, the spinels precipitated from slag are mainly multicomponent, which could have even lower Gibbs free energy of formation. Therefore, the precipitation of spinels containing Mg, Al, Cr, Zn and Fe is possible from the thermodynamic viewpoint.

Generally, spinel crystals are a class of ionic compounds formed by strongly electropositive metal ions and electronegative nonmetal ions. The stoichiometric formula of normal spinels can be AB_2X_4: divalent cation A is in a tetrahedral site, trivalent cation B is in an octahedral site, and divalent anion X is in a normal anion site.[40] However, the isomorphism replacement phenomenon in the spinel structure occurs frequently. In the present study, the decomposed Zn^{2+} could replace the Mg^{2+} in A site in the primary crystallized spinel, and Fe^{3+} could replace Cr^{3+} and Al^{3+} in B site. Thereby, Zn and Fe could have important distributions in spinel phases. The incorporation of Zn and Fe in the spinel could be further confirmed by XRD patterns. As shown in Figure 4, the 2θ position of the spinel peak was observed to shift toward a lower degree. The addition of $ZnFe_2O_4$ in slag would lead to incorporation of Zn^{2+} and Fe^{3+} in spinel. The incorporation of Zn^{2+} and

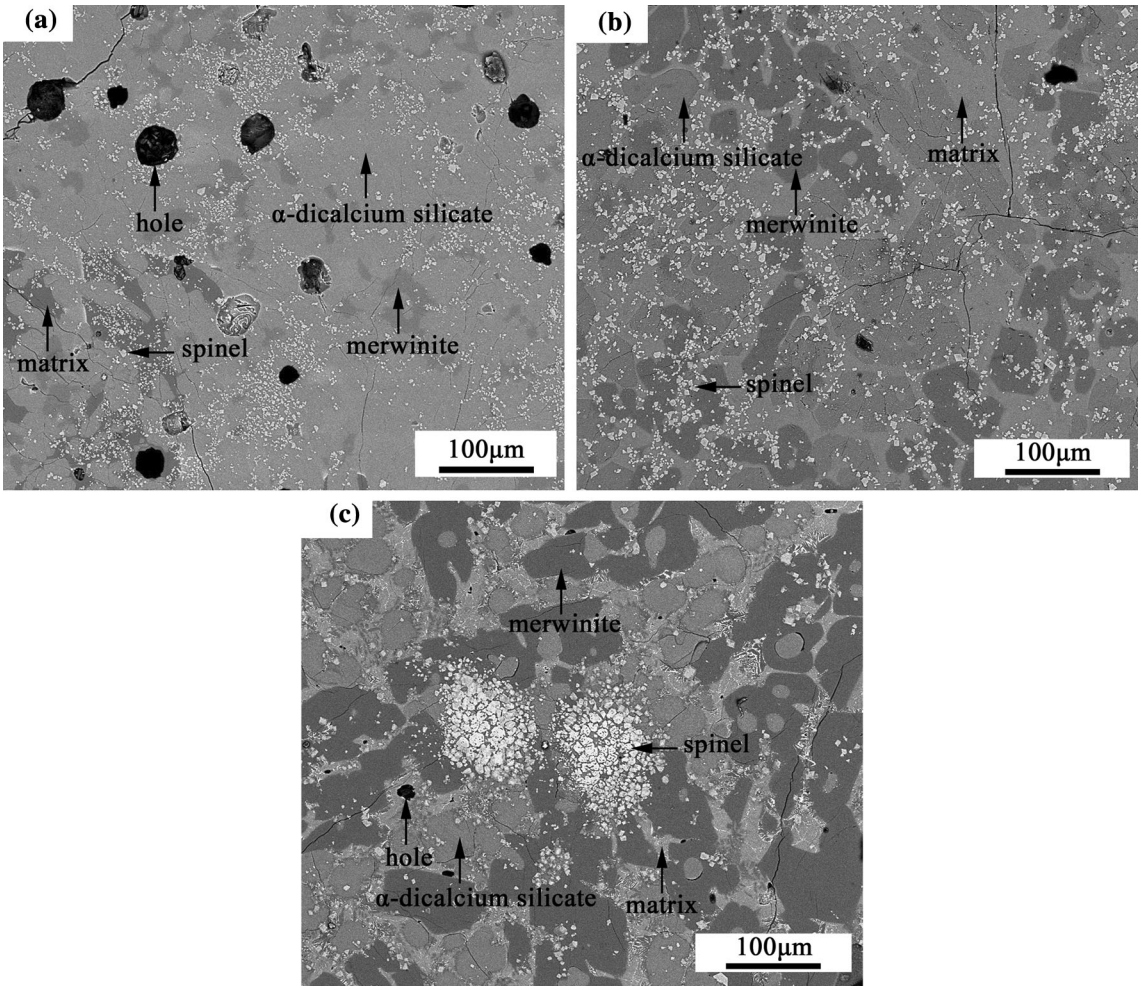

Fig. 3—SEM images of the samples with different amounts of $ZnFe_2O_4$ addition: (*a*) 0 wt pct $ZnFe_2O_4$; (*b*) 2 wt pct $ZnFe_2O_4$; (*c*) 4 wt pct $ZnFe_2O_4$.

Fe^{3+} in the spinel lattice would change the lattice parameters of the spinel structure, leading to the shift in the spinel phase diffraction peak.[41]

Figure 3 shows that the spinel phase size increased obviously with $ZnFe_2O_4$ addition. The mean sizes of the spinel measured by an image analysis software in 0 wt pct $ZnFe_2O_4$, 2 wt pct $ZnFe_2O_4$ and 4 wt pct $ZnFe_2O_4$ are 2, 6 and 13 μm, respectively. The increased size of spinel phase could be due to the enhanced crystal growth or Ostwald ripening. These two mechanisms are discussed below.

If the crystal growth of the precipitated phases in the present slag is interface-controlled, the growth rate Y depends on the viscosity of slag and Gibbs free energy between the crystal and molten slag, according to the following Eq. [42]:

$$Y = \frac{fkT}{3\pi a_0^2 \eta}\left(1 - \exp\left(-\frac{\Delta\mu}{RT}\right)\right) \quad [3]$$

where a_0 is the thickness per molecular layer, and f is the fraction of sites on the crystal surface available for attachment. $\Delta\mu$ is the Gibbs free energy between crystal and molten slag, η is the viscosity of melts, k is the Boltzmann constant, and T is the temperature in Kelvin. $\Delta\mu$ can be calculated from the undercooling degree $\Delta T = T_L - T$ according to the following equation:

$$\Delta\mu = \frac{\Delta H_C \Delta T}{T_L} \quad [4]$$

where ΔH_C is the latent heat of crystallization; T_L is the liquidus temperature. Combining Eqs. [3] with [4], we get

$$Y = \frac{fkT}{3\pi a_0^2 \eta}\left(1 - \exp\left(-\frac{\Delta H_C \Delta T}{RTT_L}\right)\right) \quad [5]$$

Equation [5] shows that the viscosity of slag plays a critical role in the crystal growth in slag. No literature was found regarding $ZnFe_2O_4$'s effects on the viscosity of slag. However, $ZnFe_2O_4$ would dissolve into slags and decompose into ions of Zn^{2+} and FeO_4^{5-} or Fe^{2+} at 1273 K. Therefore, we can consider the effect of ZnO and Fe_tO on the viscosity of slag. There are many research works on the effects of ZnO and Fe_tO on the

Table IV. Chemical Compositions of Various Mineralogic Phases for all Samples Determined by SEM-EDS (Wt Pct)

Sample	Phases	CaO	SiO_2	MgO	Al_2O_3	Cr_2O_3	Fe_2O_3	ZnO
1	α-dicalcium silicate	54.77	37.79	5.97	0.21	1.27	—	—
	merwinite	47.48	37.28	11.71	0.68	2.84	—	—
	spinel	1.19	0.59	13.00	18.25	66.97	—	—
	matrix	34.30	32.63	5.77	26.36	0.93	—	—
2	α-dicalcium silicate	54.60	37.38	5.85	0.49	0.95	1.84	0.73
	merwinite	48.73	38.54	11.31	0.26	1.15	2.04	0.63
	spinel	1.22	0.54	11.54	17.16	69.54	5.23	1.32
	matrix	38.65	34.57	4.44	20.82	1.52	5.14	0.69
3	α-dicalcium silicate	57.79	36.58	2.79	0.88	1.13	3.43	0.83
	merwinite	45.12	39.83	12.90	0.78	1.37	2.90	0.77
	spinel	1.07	0.57	12.91	3.66	82.00	6.96	2.06
	matrix	37.27	29.67	2.18	29.70	1.18	12.49	1.46

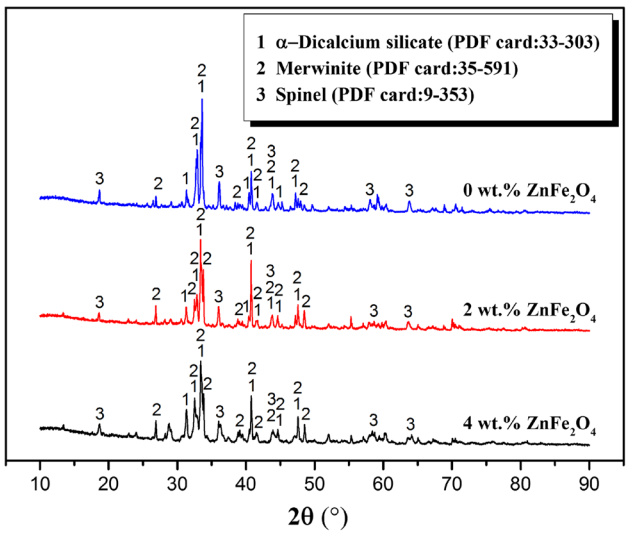

Fig. 4—XRD patterns of the samples with different amounts of $ZnFe_2O_4$ addition.

viscosity of slag. Jin *et al.*[43] investigated the effect of ZnO on the viscosity and structure of CaO-FeO-Al_2O_3-SiO_2 slag. The slag viscosity decreases continuously with increasing ZnO content from 0 to 20 wt pct. By employing Raman spectroscopy, they also found that the degree of polymerization (DOP) of the as-quenched slags decreases with increasing ZnO content, which could explain the decrease of viscosity with increasing ZnO content. Wang *et al.*[44] investigated the influence of Fe_tO on the viscosity of steelmaking slags and found that the viscosity of CaO-SiO_2-Al_2O_3-MgO-Fe_tO-P_2O_5 slags decreases with increasing Fe_tO content. Since ZnO and Fe_tO could reduce the viscosity of steelmaking slags, it is expected that $ZnFe_2O_4$ would also reduce it. Therefore, the crystal growth rate would be raised according to Eq. [5]. In other words, the introduction of $ZnFe_2O_4$ would promote the crystal growth.

Ostwald ripening is known as a process in which large crystals grow with time at the expense of the small ones in a system consisting of crystals and liquids. The driving force for Ostwald ripening is the minimization of solid-liquid interfacial energy. Based on mean field approximation method, the Lifshitz–Slyozov–Wagner (LSW) theory[45,46] can describe the kinetics of Ostwald ripening very well. The kinetics of Ostwald ripening can be controlled by the diffusion between large and small crystals in liquid or the growth or dissolution at the interface. If it is assumed that Ostwald ripening during cooling of the present slag was controlled by diffusion in liquid, we could have

$$\overline{d}^3 - \overline{d_0}^3 = \frac{64 D \sigma_{SL} V_S c_0}{9RT} t \qquad [6]$$

where $\bar{d}$is the mean crystal size at time t; $\bar{d}_0$is the initial mean crystal size; D is the effective diffusion coefficient; σ_{SL} is the solid–liquid interfacial tension; V_S is the molar volume of crystal; c_0 is the mass concentration of mobile species in liquid equilibrated with a crystal with infinitely large size.

Equation [6] shows that the ripening rate is proportional to the effective diffusion coefficient. The well-known Stokes–Einstein equation could relate the diffusion coefficient to viscosity as follows:

$$D = \frac{kT}{6\pi r \eta} \qquad [7]$$

where D is the diffusion coefficient of ions in slag; η is the viscosity of slag; T is the temperature in Kelvin; k is the Boltzmann constant; r is the radius of ions in slag.

According to Eqs. [6] and [7], the ripening rate is inversely proportional to the viscosity of slag. Since the addition of $ZnFe_2O_4$ would decrease the viscosity of the slag, the rate of Ostwald ripening in the present case would be raised with the addition of $ZnFe_2O_4$. Therefore, larger spinel crystallization could be found in samples with more $ZnFe_2O_4$ addition.

Figures 3 and 4 show that the amount and size of dicalcium silicate crystals decrease with increasing $ZnFe_2O_4$ content in slag. From Figure 2, the precipitation temperature and mass percentage of precipitated $ZnFe_2O_4$ phase decrease with increasing $ZnFe_2O_4$ content in slag. According to Eq. [5], the crystal growth rate

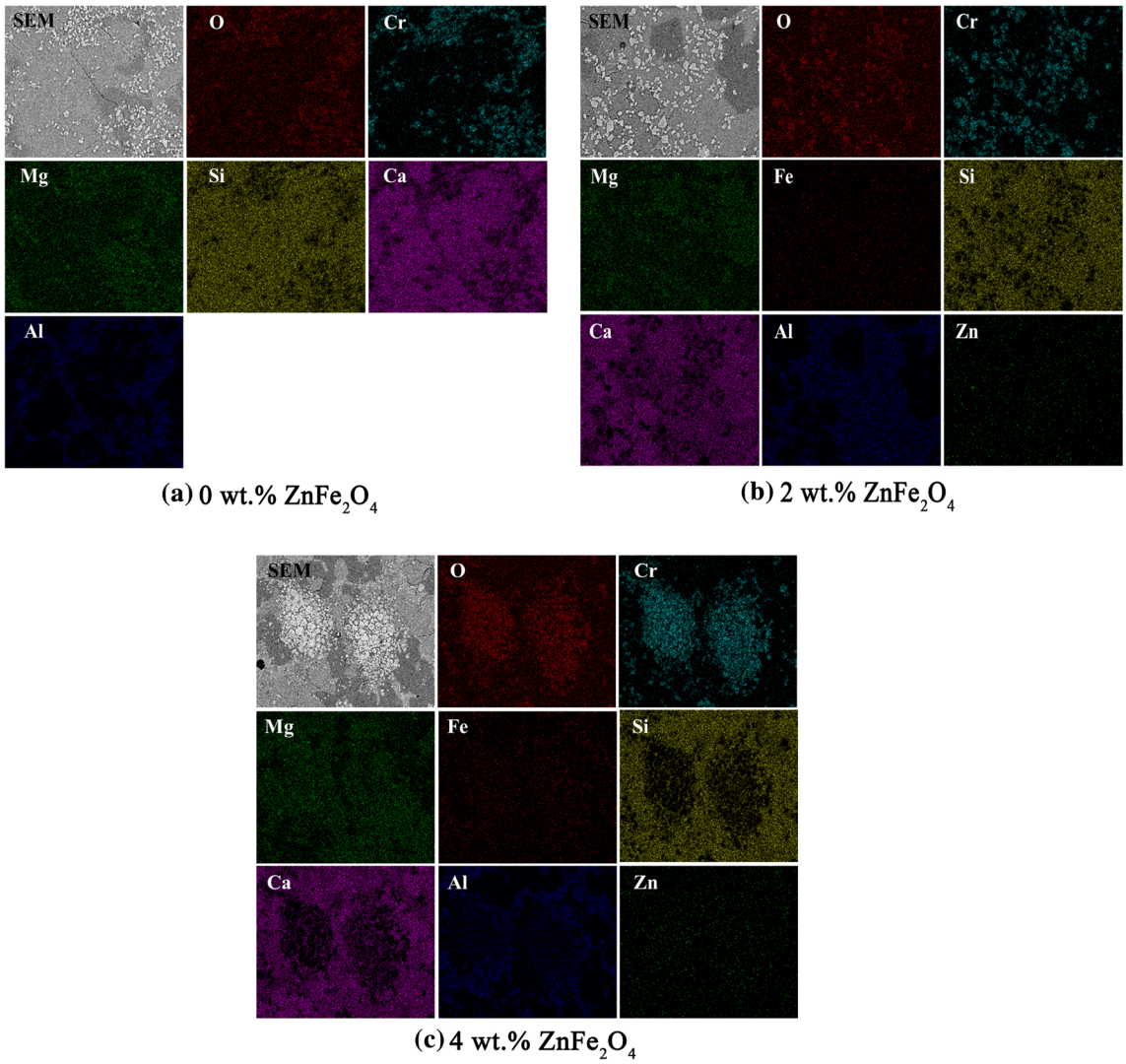

Fig. 5—Distribution diagram of elements in samples analyzed by EDS mapping: (*a*) 0 wt pct $ZnFe_2O_4$; (*b*) 2 wt pct $ZnFe_2O_4$; (*c*) 4 wt pct $ZnFe_2O_4$.

decreases as the undercooling degree decreases. Therefore, the undercooling degree for crystallization of α-Ca_2SiO_4 was reduced by increasing $ZnFe_2O_4$, leading to the suppression of crystallization of α-Ca_2SiO_4.

Figure 3 further shows that the size of merwinite crystals increases with the increase of $ZnFe_2O_4$ content in slag. The diffraction peak intensities of merwinite are enhanced in XRD patterns, shown in Figure 4. As shown in Figure 2, the precipitation temperature for merwinite decreases slightly with increasing $ZnFe_2O_4$ content. Therefore, the undercooling degree for precipitation of merwinite does not change much. The crystallization of merwinite is mainly determined by the viscosity of slag. According to Eq. [3], the rate of crystal growth is inversely proportional to the viscosity of slag. The addition of $ZnFe_2O_4$ decreases the viscosity of slag and thereby increases the crystal growth rate of merwinite in slag. Accordingly, the crystallization of merwinite was promoted by increasing $ZnFe_2O_4$ content.

B. *Leachability of Chromium and Zinc in Synthetic Stainless Slag*

Figure 7 presents the effect of $ZnFe_2O_4$ on the leaching concentration of chromium of synthetic stainless steel slag according to the US-EPA-3060A method. As the figure shows, the leaching concentrations of chromium were reduced by addition of $ZnFe_2O_4$, which were far below the chemical limits defined in the French proposal for a criterion and evaluation method for waste ecotoxicity (CEMWE) (0.1 mg L^{-1}[47]). From mineralogic phase analysis, the Zn and Fe would be incorporated into the multicomponent spinel phase in synthetic stainless steel slag. Meanwhile, the addition of $ZnFe_2O_4$ would be beneficial to the crystal growth of spinel and merwinite during cooling. It is well known that the structure of spinel is very stable and difficult to leach.[6,7] The crystallization of spinel would alleviate the leaching of chromium from slag. It was also reported that the existence of Ca_2SiO_4 enhances the leaching of chromium.[8,12] The present work showed that the

Table V. Distribution of Zn and Cr in Ca_2SiO_4, Spinel, Liquid Slag and $Ca_3MgSi_2O_8$

Sample	Phase	FactSage Simulation Results		SEM-EDS Results	
		Cr (Pct)	Zn (Pct)	Cr (Pct)	Zn (Pct)
0 Wt Pct $ZnFe_2O_4$	liquid slag	0.056	—	0.56	—
	spinel	45.651	—	42.27	—
	α-Ca_2SiO_4	—	—	0.51	—
	$Ca_3MgSi_2O_8$	—	—	0.83	—
2 Wt Pct $ZnFe_2O_4$	liquid slag	0.075	0.653	0.62	0.72
	spinel	43.424	2.650	42.78	1.91
	α-Ca_2SiO_4	—	0.060	0.22	0.56
	$Ca_3MgSi_2O_8$	—	—	0.46	0.92
4 Wt Pct $ZnFe_2O_4$	liquid slag	0.080	1.256	0.50	1.45
	spinel	41.571	4.794	49.57	2.84
	α-Ca_2SiO_4	—	0.118	0.48	0.78
	$Ca_3MgSi_2O_8$	—	—	0.49	0.70

— means not detected.

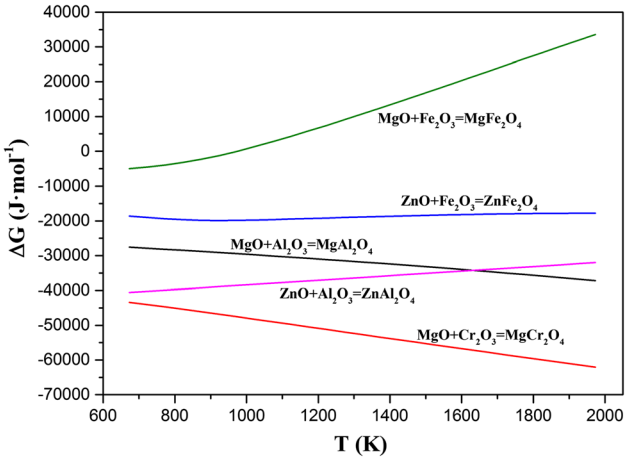

Fig. 6—Formation Gibbs free energies of binary spinels.

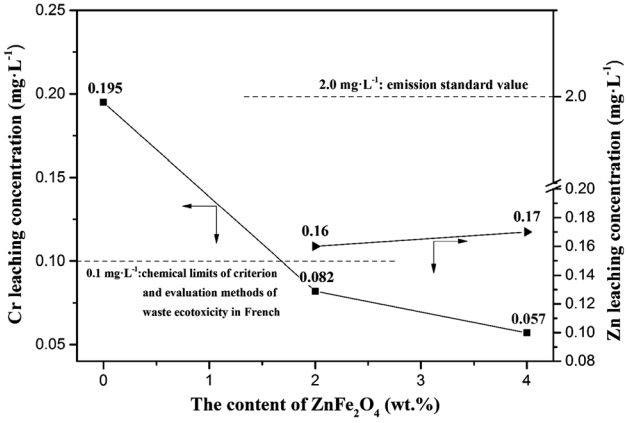

Fig. 7—Chromium and zinc leaching concentrations of synthetic slag samples.

crystallization of Ca_2SiO_4 was suppressed by the addition of $ZnFe_2O_4$, which was also beneficial to the reduction of chromium leaching from slag.

The zinc leaching concentrations of the samples with $ZnFe_2O_4$ addition were determined by the TCLP method and are also shown in Figure 7. The ICP-OES results showed that the leaching concentrations of zinc were 0.16 and 0.17 mg L^{-1} for the samples adding 2 and 4 wt pct $ZnFe_2O_4$, respectively. These values were far below the emission standard value for zinc of 2.0 mg L^{-1} (Chinese standard: GB 25466-2010[48]). Low zinc leaching concentrations indicate that ZnO was successfully incorporated in the spinel phase. Due to the stability of spinel, the Zn leachability of slag was low.

C. *Validation of Immobilization of Chromium in Stainless Steel Slag Using EAF Dusts*

It was shown that the addition of $ZnFe_2O_4$ is beneficial to the crystal growth of spinel and reduction of chromium leaching in synthetic stainless steel slag. The leaching of zinc in synthetic stainless steel slag was much lower than the limit value of zinc. All these indicate that it is feasible to employ EAF dusts for immobilization of chromium in stainless steel slag.

Based on the results obtained from synthesized slags, a synergistic treatment of industrial stainless steel slag and EAF dusts was carried out under similar experimental conditions. The mixing ratio of industrial stainless steel slag to EAF dusts was 4/1. Figure 8 shows the SEM images of initial stainless steel slag, slag after heat treatment and final slag after synergistic treatment with EAF dusts. Three mineralogic phases named α-dicalcium silicate, merwinite and spinel were determined by SEM-EDS combined with XRD patterns in Figure 9. These results are in agreement with the results for synthetic slags. The spinel in slag tends to agglomerate, and the mean size of spinel is approximate 40 μm. The distributions of chromium in various mineralogic phases in the initial stainless steel slag after heat treatment and synergistic treatment are summarized in Table VI. The content of chromium in α-Ca_2SiO_4 phase decreased significantly after heat and synergistic treatment. Figure 10 presents the leaching concentrations of chromium in initial industrial

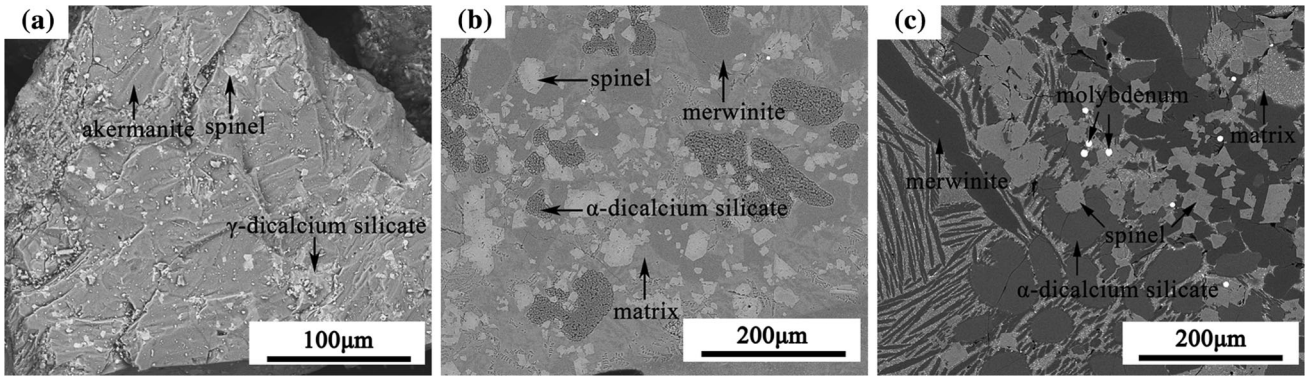

Fig. 8—SEM images of (*a*) initial stainless steel slag, (*b*) slag after heat treatment and (*c*) final slag after synergistic treatment with EAF dusts.

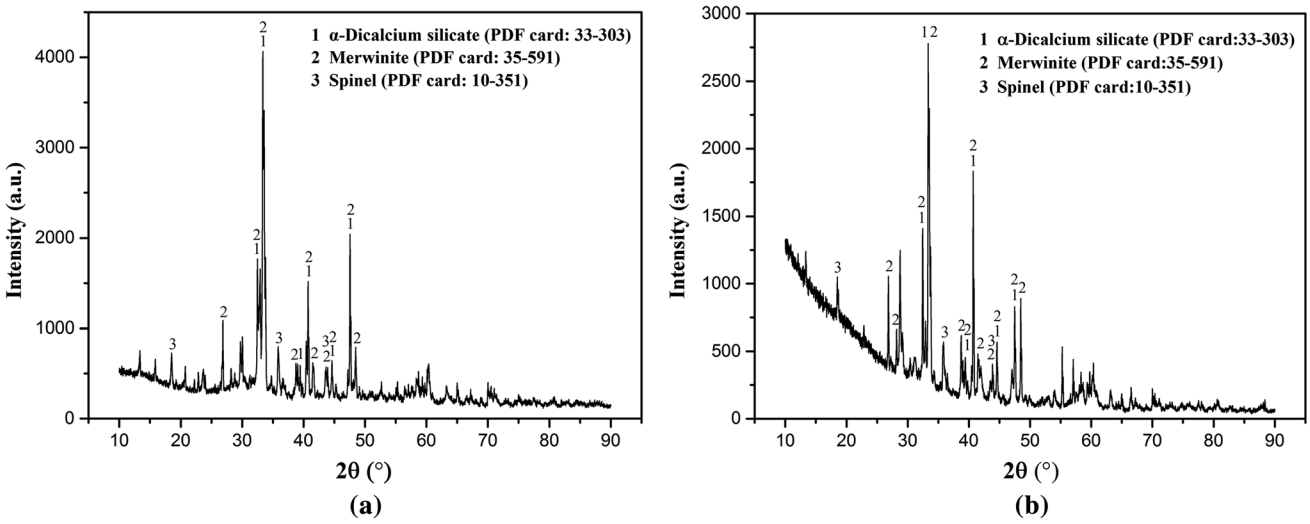

Fig. 9—XRD patterns of (*a*) industrial stainless steel slag after heat treatment and (*b*) final slag after synergistic treatment with EAF dusts.

stainless steel slag and samples after heat treatment with and without EAF dusts addition. The leaching concentration of chromium in initial industrial stainless steel slag was 0.347 mg L^{-1}. After heat treatment using the present temperature regime, the leaching concentration of chromium deceased to 0.046 mg L^{-1}. The leaching concentration of chromium further decreased with the addition of EAF dusts. No leaching concentration of chromium was detected in the filtrate within the accuracy of the ICP-MS. This decreasing trend in industrial samples is consistent with that of synthetic samples. As we discussed in Sect. III–B, the presence of Ca_2SiO_4 would enhance the leaching of chromium.[8,12] Therefore, the reduction of chromium content in Ca_2SiO_4 phase is beneficial to the suppression of the leaching of chromium. As for initial EAF dusts, the zinc leaching concentration was 3.09 mg L^{-1}, which exceeds the emission standard value (2.0 mg L^{-1}[48]). However, the zinc leaching concentration decreased sharply to 0.85 mg L^{-1} after synergistic treatment. Accordingly, synergistic treatment of stainless steel slag and EAF dusts is beneficial for immobilizing chromium in stainless steel slag. The leaching concentration of zinc in the final slag is below the emission standard value. The final slag after treatment meets the sanitary landfill standard.

D. *Technologic Route of the Synergistic Treatment Method*

The above experimental results demonstrated that synergistic treatment of stainless steel slag and EAF dusts was effective for chromium immobilization. The final slag can be disposed of by sanitary landfilling or recycling as constructional materials in view of its low metal leaching. A schematic technologic route diagram of synergistic treatment is given in Figure 11. Prior to discharging stainless steel slag, the collected EAF dusts from dust cleaning systems are pelletized and loaded into an empty ladle according to the appropriate proportion. The melting stainless steel slag discharges into the ladle furnace directly and mixes with pelletized EAF dusts. The ladle furnace can be covered and heated using graphite electrodes afterwards. After that, the final slags can be poured and naturally cooled in slag yards. Besides, methods of mitigating Zn volatilization need to

Table VI. Distribution of Cr in the Initial Sample, After Heat and Synergistic Treatment

Phases	Initial Stainless Steel Slag (Pct)	After Heat Treatment (Pct)	After Synergistic Treatment with EAF Dusts Addition (Pct)
α-Dicalcium silicate	1.57	0.24	0.47
Merwinite	—	0.71	0.65
Spinel	47.33	53.08	48.0
Matrix	0.31	0.86	0.76

— means not detected.

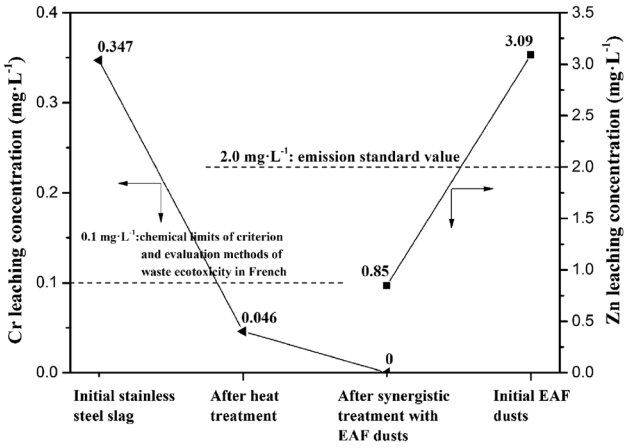

Fig. 10—Chromium and zinc leaching concentration of industrial materials.

be considered in view of different Zn-containing phases. The volatilization of ZnO could be largely avoided by the dissolution of EAF dusts in molten stainless steel slag. It has been shown that the volatilization of ZnO in stainless steel slag can be weak. During cooling, the Zn is mainly enriched in spinel phase, which has a high melting point and hardly volatilizes. However, many technical details, such as the quality ratio of stainless steel slag and EAF dusts and the dissolution of dust pellets into stainless slag, need to be studied in the future.

IV. CONCLUSIONS

To immobilize chromium in stainless steel slag effectively, a synergistic treatment of stainless steel slag and EAF dusts was proposed in this work. The effect of $ZnFe_2O_4$ addition on the mineralogic phases of synthetic $CaO\text{-}SiO_2\text{-}MgO\text{-}Al_2O_3\text{-}Cr_2O_3$ slag was investigated first to explore the feasibility of the present method. SEM-EDS and XRD measurements were employed to determine the phase composition. Furthermore, the leaching concentrations of chromium and zinc were evaluated according to the US-EPA-3060A method and TCLP method 1311, respectively. Finally, validation of the present method was carried out on industrial stainless steel slag and EAF dusts. The following conclusions could be drawn:

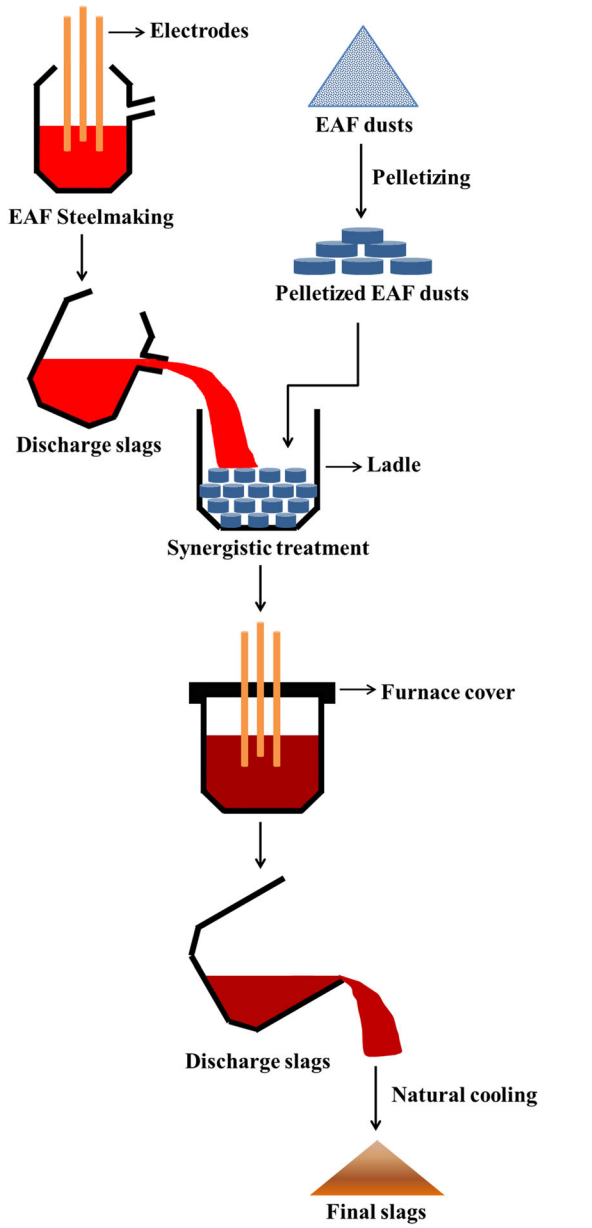

Fig. 11—Schematic technologic route diagram of synergistic treatment.

1. Three crystalline phases were identified in the sample without $ZnFe_2O_4$ addition: α-di-calcium silicate, merwinite and spinel phase. The main crystalline

phases remained unchanged in the samples with 2 and 4 wt pct $ZnFe_2O_4$ addition.
2. The crystallization of spinel and merwinite phases was enhanced by the addition of $ZnFe_2O_4$ but suppressed the precipitation of α-Ca_2SiO_4.
3. The leaching concentrations of chromium were decreased by the addition of $ZnFe_2O_4$, indicating that $ZnFe_2O_4$ can be used to immobilize chromium in stainless steel slag. The zinc leaching concentrations of the samples with $ZnFe_2O_4$ addition were far below the emission standard value.
4. Synergistic treatment of stainless steel slag and EAF dusts is beneficial to immobilize chromium in stainless steel slag. The leaching concentration of zinc in the final slag is below to the emission standard value. The final slag after treatment meets the sanitary landfill standard.

ACKNOWLEDGMENTS

Open access funding provided by University of Oulu including Oulu University Hospital.

FUNDING

This work was supported by the Natural Science Foundation of China (NSFC contract nos. 51774026, 51534001, 51774025) and the Academy of Finland for Genome of Steel Grant (No. 311934).

CONFLICT OF INTEREST

None.

OPEN ACCESS

REFERENCES

1. H. Zhang and X. Hong: *Resour. Conserv. Recycl.*, 2011, vol. 55, pp. 745–54.
2. K. Pillay, H.V. Blottnitz, and J. Petersen: *Chemosphere*, 2003, vol. 52, pp. 1771–79.
3. C.J. Chan, W.M. Kriven, and J.F. Young: *J. Am. Ceram. Soc.*, 1992, vol. 75, pp. 1621–27.
4. M. Tossavainen, F. Engstrom, Q. Yang, N. Menad, M.L. Larsson, and B. Bjorkman: *Waste Manag.*, 2007, vol. 27, pp. 1335–44.
5. A.M. Fällman: *Waste Manag.*, 2000, vol. 20, pp. 149–54.
6. M. Loncnar, M. Zupančič, P. Bukovec, and A. Jaklič: *Mater. Technol.*, 2009, vol. 43, pp. 315–21.
7. L.A. Díaz, R. Torrecillas, AHD. Aza, and P. Pena: *J. Eur. Ceram. Soc.*, 2007, vol. 27, pp. 4623–31.
8. H. Cabrera-Real, A. Romero-Serrano, B. Zeifert, A. Hernandez-Ramirez, M. Hallen-López, and A. Cruz-Ramirez: *J. Mater. Cycles Waste Manag.*, 2012, vol. 14, pp. 317–24.
9. C. Martinez-Morales, A. Romero-Serrano, B. Zeifert, A. Hernandez-Ramirez, A. Cruz-Ramirez, and M. Perez-Labra: *Trans. Indian Inst. Met.*, 2017, vol. 70, pp. 1399–1407.
10. G.J. Albertsson, L.D. Teng, F. Engström, and S. Seetharaman: *Metall. Mater. Trans. B*, 2013, vol. 44B, pp. 1586–97.
11. G.J. Albertsson, L.D. Teng, and B. Björkman: *Miner. Process. Extr. Metall.*, 2014, vol. 123, pp. 116–22.
12. Q.F. Shu, Q.Y. Luo, L.J. Wang, and K. Chou: *Steel Res. Int.*, 2015, vol. 86, pp. 391–99.
13. E. García-Ramos, A. Romero-Serrano, B. Zeifert, P. Flores-Sánchez, M. Hallen-López, and E.G. Palacios: *Steel Res. Int.*, 2008, vol. 79, pp. 332–39.
14. J.L. Li, A.J. Xu, D.F. He, Q.X. Yang, and N.Y. Tian: *Int. J. Miner. Metall. Mater.*, 2013, vol. 20, pp. 253–58.
15. R.I. Iacobescu, A. Malfliet, L. Machiels, P.T. Jones, B. Blanpain, and Y. Pontikes: *Waste Biomass Valor.*, 2014, vol. 5, pp. 343–53.
16. A.G. Guézennec, J.C. Huber, F. Patisson, P. Sessiecq, J.P. Birat, and D. Ablitzer: *Powder Technol.*, 2005, vol. 157, pp. 2–11.
17. S. Itoh, A. Tsubone, K. Matsubae-Yokoyama, K. Nakajima, and T. Nagasaka: *ISIJ Int.*, 2008, vol. 48, pp. 1339–44.
18. JGMS. Machado, F.A. Brehm, C.A.M. Moraes, C.A.D. Santos, A.C.F. Vilela, and J.B.M.D. Cunha: *J. Hazard. Mater.*, 2006, vol. 136, pp. 953–60.
19. T. Sofilić, A. Rastovčan-Mioč, Š. Cerjan-Stefanović, V. Novosel-Radović, and M. Jenko: *J. Hazard. Mater.*, 2004, vol. 109, pp. 59–70.
20. M.K. Jha, V. Kumar, and R.J. Singh: *Resour. Conserv. Recycl.*, 2001, vol. 33, pp. 1–22.
21. R. Chairaksa-Fujimoto, Y. Inoue, N. Umeda, S. Itoh, and T. Nagasaka: *Int. J. Miner. Metall. Mater.*, 2015, vol. 22, pp. 788–97.
22. K. Mager, U. Meurer, and J. Wirling: *JOM*, 2003, vol. 55, pp. 20–25.
23. G. Orhan: *Hydrometallurgy*, 2005, vol. 78, pp. 236–45.
24. T. Havlík, B.V. Souza, A.M. Bernardes, I.A.H. Schneider, and A. Miškufová: *J. Hazard. Mater.*, 2006, vol. 135, pp. 311–18.
25. R. Chairaksa-Fujimoto, K. Maruyama, T. Miki, and T. Nagasaka: *Hydrometallurgy*, 2016, vol. 159, pp. 120–25.
26. C.F. Pereira, M. Rodriguez-Pinero, and J. Vale: *J. Hazard. Mater.*, 2001, vol. 82, pp. 183–95.
27. O. Ruiz, C. Clemente, M. Alonso, and F.J. Alguacil: *J. Hazard. Mater.*, 2007, vol. 141, pp. 33–36.
28. H.G. Wang, J.M. Gao, W.W. Liu, M. Zhang, and M. Guo: *Hydrometallurgy*, 2016, vol. 166, pp. 1–8.
29. U.S. EPA. United States Environmental Protection Agency. SW-846 Method 3060A: Test methods for evaluating solid wastes, Physical/Chemical Methods, https://www.epa.gov/hw-sw846/sw-846-test-method-3060a-alkaline-digestion-hexavalent-chromium. Accessed Dec 1996.
30. U.S. EPA. United States Environmental Protection Agency. SW-846 Method 1311: Toxicity characterisation leaching procedure (TCLP), https://www.epa.gov/hw-sw846/sw-846-test-method-1311-toxicity-characteristic-leaching-procedure. Accessed Jul 1992.
31. C.W. Bale, P. Chartrand, S.A. Degterov, G. Eriksson, K. Hack, R.B. Mahfoud, J. Melançon, A.D. Pelton, and S. Petersen: *Calphad*, 2002, vol. 26, pp. 189–228.
32. D. Durinck, P.T. Jones, B. Blanpain, P. Wollants, G. Mertens, and J. Elsen: *J. Am. Ceram. Soc.*, 2007, vol. 90, pp. 1177–85.
33. C.L. Yaws: *Handbook of Vapor Pressure: Inorganic Compounds and Elements*, Gulf Publishing Co., Houston, 1995, vol. 4.

34. P. Segui, J.E. Aubert, B. Husson, and M. Measson: *Appl. Clay Sci.*, 2012, vol. 57, pp. 79–85.
35. C.E. Tilley and H.C.G. Vincent: *Miner. Mag. J. Miner. Soc.*, 1948, vol. 28, pp. 255–71.
36. D. Moseley and F.P. Glasser: *Cem. Concr. Res.*, 1981, vol. 11, pp. 559–65.
37. K.H. Lee, S.H. Park, H.S. Yoon, Y. Kim, H.G. Jang, and W.B. Im: *Opt. Express*, 2012, vol. 20, pp. 6248–57.
38. J. Bai, A. Chaipanich, JM. Kinuthia, M. O'Farrell, BB. Sabir, S. Wild, and M.H. Lewis: *Cem. Concr. Res.*, 2003, vol. 33, pp. 1189–1202.
39. V.D. Tathavakar, M.P. Antony, and A. Jha: *Metall. Mater. Trans. B*, 2005, vol. 36B, pp. 75–84.
40. W.L. Li and X.X. Xue: *Ironmak. Steelmak.*, 2019, vol. 46, pp. 642–48.
41. C.Z. Liao, Y.Y. Tang, C.S. Liu, K. Shih, and F.B. Li: *J. Hazard. Mater.*, 2016, vol. 311, pp. 246–53.
42. R.J. Kirkpatrick: *Am. Miner. J. Earth Planet. Mater.*, 1975, vol. 60, pp. 798–814.
43. Z.N. Jin, H.Y. Yang, J.F. Lv, L.L. Tong, G.B. Chen, and Q. Zhang: *JOM*, 2018, vol. 70, pp. 1430–36.
44. Z.J. Wang, Q.F. Shu, S. Sridhar, M. Zhang, M. Guo, and Z.T. Zhang: *Metall. Mater. Trans. B*, 2015, vol. 46B, pp. 758–65.
45. I.M. Lifshitz and V.V. Slyozov: *J. Phys. Chem. Solids*, 1961, vol. 19, pp. 35–50.
46. C. Wagner: *Z. Elektrochem. Ber. Bunsenges. Phys. Chem.*, 1961, vol. 65, pp. 581–91.
47. French Ministry of Environment/Directorate for Prevention Pollution and Risk Control/ Products and Division of Wastes (Eds). Proposal for a Criterion and Evaluation Methods of Waste Ecotocixity. Paris, 1998.
48. Standardization Administration of the People's Republic of China. The National Standard of the People's Republic of China, GB 25466-2010: Emission standard of pollutants for lead and zinc industry. http://www.gb688.cn/bzgk/gb/newGbInfo?hcno=58F6F8492620D025A04DE7393C122658. Accessed 10 Nov. 2010.